# Image Copy-Move Forgery Detection using Color Features and Hierarchical Feature Point Matching

Yi-Lin Tsai and Jin-Jang Leou
*Department of Computer Science and Information Engineering, National Chung Cheng University, Chiayi 621, Taiwan*

Keywords: Copy-Move Forgery Detection, Hierarchical Feature Point Matching, Color Feature, Iterative Forgery Localization.

Abstract: In this study, an image copy-move forgery detection approach using color features and hierarchical feature point matching is proposed. The proposed approach contains three main stages, namely, pre-processing and feature extraction, hierarchical feature point matching, and iterative forgery localization and post-processing. In the proposed approach, Gaussian-blurred images and difference of Gaussians (DoG) images are constructed. Hierarchical feature point matching is employed to find matched feature point pairs, in which two matching strategies, namely, group matching via scale clustering and group matching via overlapped gray level clustering, are used. Based on the experimental results obtained in this study, the performance of the proposed approach is better than those of three comparison approaches.

## 1 INTRODUCTION

Copy-move forgery, a common type of forged images, copies and pastes one or more regions onto the same image (Cozzolino, Poggi, and Verdoliva, 2015). Some image processing operations, such as transpose, rotation, scaling, and JPEG compression, will make images more convincing. To deal with copy-move forgery detection (CMFD), many CMFD approaches have been proposed, which can be roughly divided into three categories: block-based, feature point-based, and deep neural network based.

Cozzolino, Poggi, and Verdoliva (2015) used circular harmonic transform (CHT) to extract image block features. A fast approximate nearest-neighbor search approach (called patch match) is used to deal with invariant features efficiently. Fadl and Semary (2017) proposed a block-based CMFD approach using Fourier transform for feature extraction. Bi, Pun, and Yuan (2016) proposed a CMFD approach using hierarchical feature matching and multi-level dense descriptor (MLDD).

Amerini, et al. (2011) proposed a feature point-based CMFD approach using scale invariant feature transform (SIFT) (Lowe, 2004) for feature point extraction. Amerini, et al. (2013) developed a CMFD approach based on J-linkage, which can effectively solve the problem of geometric transformation. Pun, Yuan, and Bi (2015) proposed a CMFD approach using feature point matching and adaptive oversegmentation. Warif, et al. (2017) proposed a CMFD approach using symmetry-based SIFT feature point matching. Silva, et al. (2015) presented a CMFD approach using multi-scale analysis and voting processes. Jin and Wan (2017) proposed an improved SIFT-based CMFD approach. Li and Zhou (2019) developed a CMFD approach using hierarchical feature point matching. Huang and Ciou (2019) proposed a CMFD approach using superpixel segmentation, Helmert transformation, and SIFT feature point extraction (Lowe, 2004). Chen, Yang, and Lyu (2020) proposed an efficient CMFD approach via clustering SIFT keypoints and searching the similar neighborhoods to locate tampered regions.

Zhong and Pun (2020) proposed a CMFD scheme using a Dense-InceptionNet. Dense-InceptionNet is an end-to-end multi-dimensional dense-feature connection deep neural network (DNN), which consists of pyramid feature extractor, feature correlation matching, and hierarchical post-processing modules. Zhu, et al. (2020) proposed a CMFD approach using an end-to-end neural network based on adaptive attention and residual refinement network (AR-Net). Islam, Long, Basharat, and Hoogs (2020) proposed a generative adversarial network with a



Tsai, Y. and Leou, J.
Image Copy-Move Forgery Detection using Color Features and Hierarchical Feature Point Matching.
DOI: 10.5220/0010492301530159
In *Proceedings of the International Conference on Image Processing and Vision Engineering (IMPROVE 2021)*, pages 153-159
ISBN: 978-989-758-511-1

dual-order attention model to detect and locate copy-move forgeries. In this study, an image copy-move forgery detection approach using color features and hierarchical feature point matching is proposed.

This paper is organized as follows. The proposed image copy-move forgery detection approach is described in Section 2. Experimental results are addressed in Section 3, followed by concluding remarks.

# 2 PROPOSED APPROACH

## 2.1 System Architecture

As shown in Figure 1, in this study, an image copy-move forgery detection approach using color features and hierarchical feature point matching is proposed. The proposed approach contains three main stages, namely, pre-processing and feature extraction, hierarchical feature point matching, and iterative forgery localization and post-processing.

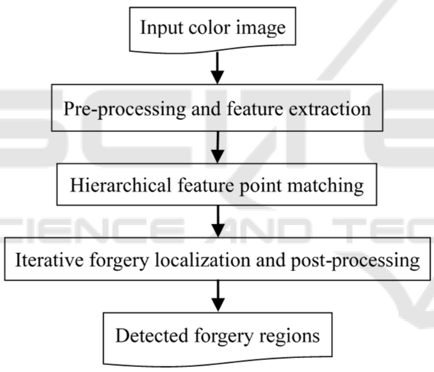


Figure 1: Framework of the proposed approach.

## 2.2 Pre-processing and Feature Extraction

Let $A_f(x, y)$, $1 \leq x \leq M$, $1 \leq y \leq N$, be the input RGB color image with size $M \times N$. The input color image will be converted from RGB color space to HSI color space and the intensity component image (I) is enhanced by histogram equalization, which is converted from HSI color space back to RGB color space, denoted as $A_{RGB}(x, y)$, $1 \leq x \leq M$, $1 \leq y \leq N$. To extract enough feature points, in this study, $A_{RGB}(x, y)$ is enlarged by $2 \times 2$ linear interpolation, denoted as $E_{RGB}(x, y)$, $1 \leq x \leq 2M$, $1 \leq y \leq 2N$. Then, image $E_{RGB}(x, y)$ is converted into gray-level image $E_{gray}(x, y)$, $1 \leq x \leq 2M$, $1 \leq y \leq 2N$, which is convolved with Gaussian filters of different scales. Gaussian-blurred image $L(x, y, m^{\alpha}\sigma)$, $1 \leq x \leq 2M$, $1 \leq y \leq 2N$, is computed as

$$L(x, y, m^{\alpha}\sigma) = G(x, y, m^{\alpha}\sigma) \otimes E_{gray}(x, y), \quad \alpha = 0, 1, \ldots, 4, \tag{1}$$

where $G(x, y, m^{\alpha}\sigma)$ denotes the Gaussian kernel, $m$ is a constant (here, $m = \sqrt{2}$), $\otimes$ denotes the convolution operator, and $\sigma$ denotes a prior smoothing value (here, $\sigma = 1.6$). Difference of Gaussians (DoG) image $D(x, y, m^{\beta}\sigma)$, $1 \leq x \leq 2M$, $1 \leq y \leq 2N$, is computed as

$$D(x, y, m^{\beta}\sigma) = L(x, y, m^{\beta+1}\sigma) - L(x, y, m^{\beta}\sigma), \quad \beta = 0, 1, 2, 3. \tag{2}$$

As multiple octaves shown in Figure 2 (Lowe, 2004), each octave contains five Gaussian-blurred images and four DoG images. The first scale value of the i-th octave is $m^{2(i-1)}\sigma$. The first octave size is $2M \times 2N$, the second octave size with down-sampling is $M \times N$, …, etc.

Within an octave, to detect the local maxima and minima of $D(x, y, m^{\beta}\sigma)$, if the value of a pixel larger (or smaller) than those of its 8 neighbors in the same image and those of $2 \times 9$ neighbors in the two neithboring DoG images with different scales, this pixel is detected as a feature point. Note that the first and last DoG images in each octave do not have feature points.

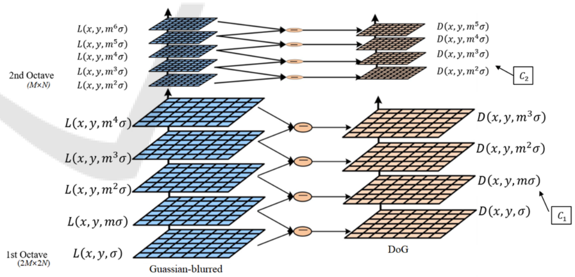


Figure 2: Illustrated schematic diagram of Gaussian-blurred images and DoG images (Lowe, 2004).

Second, using edge and contrast thresholds, all candidate feature points will be refined so that unstable extrema in SIFT feature points can be filtered out. The extrema value is computed as

$$D(\hat{F}) = D + \frac{1}{2}\left(\frac{\partial D}{\partial F}\right)^{T} \hat{F}, \tag{3}$$

$$\hat{F} = -\frac{\partial^2 D}{\partial F^2}^{-1} \times \frac{\partial D}{\partial F}, \tag{4}$$

where $F = (x, y, \sigma)^T$ and $T$ is a transpose. All extrema with $|D(\hat{x})|$ being less than $Z_h$ (set to 0.1) are discarded.

Third, to achieve rotational invariance, a gradient magnitude $\mu(x, y, m^{\beta}\sigma)$ and a guiding direction $\theta(x, y, m^{\beta}\sigma)$ defined as

$$\mu(x, y, m^{\beta}\sigma) = \sqrt{{d_x}^2 + {d_y}^2}, \tag{5}$$

$$\theta(x, y, m^{\beta}\sigma) = \tan^{-1}(d_y/d_x), \tag{6}$$

$$d_x = D(x+1,\ y,\ m^{\beta}\sigma) - D(x-1, y, m^{\beta}\sigma), \tag{7}$$

$$d_y = D(x, y+1, m^{\beta}\sigma) - D(x, y-1, m^{\beta}\sigma), \tag{8}$$

are allocated to each subsisted feature point. A generic SIFT feature point $P_k$ can be described as a four-dimensional vector, i.e.,

$$\boldsymbol{P_k = (x_k, y_k, m^s\sigma, \theta_k),\ k = 1,\ 2,\ \ldots,\ n,} \tag{9}$$

where $(x_k, y_k)$ denotes feature point coordinate, $n$ denotes the total number of feature points, and $m^s\sigma$ and $\theta_k$ denote the scale and guiding direction of $P_k$, reprectively.

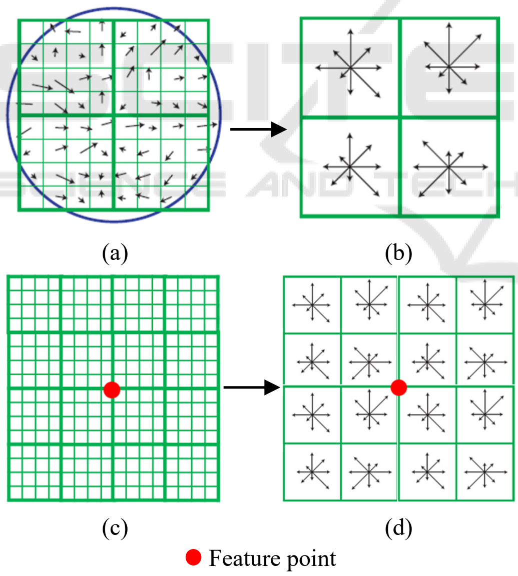


Figure 3: Schematic diagram of feature point descriptor (Lowe, 2004): (a) gradient magnitudes and guiding directions in a 8×8 region around a central feature point, (b) a 2×2 descriptor, (c) a 16×16 region around a central feature point, (d) a 128-dimensional descriptor.

As shown in Figure 3, an eight-direction histogram is formed from gradient magnitudes and guiding directions of feature points within a $4 \times 4$ region, which has 8 quantized histogram entries covering $360^{\circ}$ with the length of each arrow denoting its gradient magnitude. In a $16 \times 16$ region around a central feature point, 16 eight-direction histograms are generated, resulting in 128-dimensional $(16 \times 8)$ row vector descriptors $\omega_k = (\omega_{k,1}, \omega_{k,2}, \ldots, \omega_{k,128})$, $k = 1, 2, \ldots, n$. For $P_k$, let $ED_k$, $k = 1, 2, \ldots, n-1$ denote the Euclidean distances between descriptor $\omega_k$ and other $(n-1)$ descriptors. Let ratio R be defined as

$$\boldsymbol{R = ED^1/ED^2}, \tag{10}$$

where $ED^1$ and $ED^2$ denote the smallest and second-smallest Euclidean distances, respectively. If ratio $R$ is less than threshold $Z_t$ ($Z_t = 0.6$), feature point $P^1$ having the smallest Euclidean distance $ED^1$ is a matching feature point of $P_k$. $P_k$, $k = 1, 2, \ldots, n$ having a matching feature point as well as its matching feature point, i.e., a matching feature point pair, will be kept; otherwise, it is discarded.

## 2.3 Hierarchical Feature Point Matching

In this study, a modified version of hierarchical feature point matching (Li and Zhou, 2019) is employed, in which two matching strategies, namely, group matching via scale clustering and group matching via overlapped gray level clustering, are used.

Because Gaussian-blurred images are grouped by octave, feature points detected in different scales will be clustered closely, which can be separately processed. In this study, matching procedures are performed separately in each single high-resolution octave and jointly in multiple low-resolution octaves. Note that feature points in high-resolution octaves are much sparse than feature points in low-resolution octaves. In addition, feature points in low-resolution octaves having higher recognition capabilities can strongly resist large-scale resizing attack.

Based on the scale values, remaining feature points are divided into three categories: $C_1 = \{P_k | \, \gamma_1 \le m^s\sigma < \gamma_2\}$, $C_2 = \{P_k | \, \gamma_2 \le m^s\sigma < \gamma_3\}$, $C_3 = \{P_k | \, m^s\sigma \ge \gamma_3\}$, where $\gamma_i$ denotes the scale value of the second DoG image in the i-th octave. Note that $C_1$ contains the first octave, $C_2$ contains the second octave, and $C_3$ contains the other octaves. Feature point matching schemes are performed separately on $C_1, C_2$, and $C_3$.

Because any feature point $P_k$ and its matching feature point $P^1$ have similiar pixel values, feature points in cluster $C_i$, $i = 1,2,3$, can divided into several overlapped ranges by pixel (gray) values. In this study, the range [0, 1, …, 255] of pixel (gray) values is split into $U$ overlapped ranges,

$$U = \left\lceil \frac{255 - c_1}{c_1 - c_2} \right\rceil + 1, \quad (11)$$

where $c_1$ denotes a range size and $c_2$ denotes an overlapped size ($c_1 > c_2$). Let

$$C_{i,j} = \{P_k | \; a_i \le G_r(P_k) < b_i, P_k \in C_i\}, \\ j = 1,2,\dots,U, \quad (12)$$

$$a_i = (j-1) \times (c_1 - c_2), \quad (13)$$

$$b_i = min(a_i + c_1, \; 255), \quad (14)$$

where $G_r(P_k)$ denotes the average gray value of 9 pixels in a $3 \times 3$ region centered at $P_k$. Then, feature point matching schemes are performed separately in $C_{i,j}$, $i = 1,2,3$, $j = 1,2,\dots,U$. Let

$$Q = \bigcup Q_{i,j} \;, \; i \in \{1,\; 2,\; 3\},\; j = 1,\; 2,\; \dots,\; U, \quad (15)$$

where $Q_{i,j}$ denotes the set containing the matched feature point pairs of $C_{i,j}$.

## 2.4 Iterative Forgery Localization and Post-processing

For feature point-based copy-move forgery detection, we face two problems. First, when multiple replications are performed, the homography is usually not unique and the number of repeated areas is uncertain. Second, all matched feature point pairs usually have no matching orders, and the original and forged points are usually not distinguished by feature point matching. In this study, a modified version of iterative localization (Li and Zhou, 2019) without segmentation and clustering processes is employed, which contains four steps: elimination of isolated matched feature point pairs, estimation of local homography, homography verification and inlier selection, and forgery localization using color information and scale.

Because copy-move forgery is usually performed in a continuous shape, isolated matched feature point pairs can be detected. For each matched feature point pair $(P_k, P_{k'}) \in Q$, if $N_k$ and $N_{k'}$ denote the numbers of neighboring matched feature points for $P_k$ and $P_{k'}$ with distances being smaller than a threshold $Z_o$ (here, $Z_o = 100$), the matched feature point pair $(P_k, P_{k'})$ will be discarded if $\max\{N_k, N_{k'}\} < 2$. If $\mathcal{M}$ denotes the set containing the remaining matched feature point pairs $\in Q$, in this study, a portion of matched pairs for two consecutive local regions will be used to appraise an affine matrix. First, a matched feature point pair $(P_k, P_{k'}) \in \mathcal{M}$ is randomly selected, then all the neighboring matched feature points closed to $P_k$ and $P_{k'}$ are recorded as $E_k$ and $E_{k'}$, respectively, i.e.,

$$E_k = \{P_q | \forall P_q \in \mathcal{M},\; ED(P_q, P_k) < Z_w\}, \quad (16)$$

$$E_{k'} = \{P_q | \forall P_q \in \mathcal{M},\; ED(P_q, P_{k'}) < Z_w\}, \quad (17)$$

where $Z_w$ denotes a hyper-parameter ($Z_w = 100$) and $ED(\cdot)$ returns the Euclidean distance. Let $\mathcal{M}_k$ denote the set containing all the matched feature point pairs close to $(P_k, P_{k'}) \in \mathcal{M}$. Then, RANSAC algorithm (Gonzalez and Woods, 2018) is employed to estimate homography $H_k$ between the correspondences of matched feature point pairs in $\mathcal{M}_k$.

To delete incorrect homography estimations, a homography verification and inlier selection approach using guiding direction $\theta_k$ obtained in SIFT feature point extraction is employed. The guiding direction difference $\theta_{k'} - \theta_k$ should be consistent with the estimated affine homography $H_k$ for each proper matched feature point pair $(P_k, P_{k'})$. The matched feature point pair $(P_k, P_{k'})$ should be discarded, if

$$g(P_k, P_{k'}, H_k) = |\theta_{k'} - \theta_k - \theta_H| \le Z_\theta, \quad (18)$$

where $\theta_H$ is the estimated rotation calculated from $H_k$ and $Z_\theta$ denotes a threshold (here, $Z_\theta = 15$). Let $\widehat{\mathcal{M}}_k$ denotes the set containing the remaining matched feature point pairs in $\mathcal{M}_k$ after RANSAC homography verification. A matched feature point pair $P_k(x_k, y_k)$ and $P_{k'}(x_{k'}, y_{k'})$, will be related by

$$\begin{pmatrix} x'_k \\ y'_k \\ 1 \end{pmatrix} \approx H_k \begin{pmatrix} x_k \\ y_k \\ 1 \end{pmatrix}. \quad (19)$$

Using guiding information, set $\mathcal{M}_H$ is defined as

$$\mathcal{M}_H = \{\langle P_k, P_{k'} \rangle | \|H_k P_k - P_{k'}\|_2^2 \\ < \epsilon, g(P_k, P_{k'}, H_k) \le Z_\theta\}. \quad (20)$$

The improved homography $\widehat{H}_k$ is defined as

$$\widehat{H}_k = \underset{\widehat{H}_k}{\operatorname{argmin}} \sum_{\langle P_k, P_{k'} \rangle} \left\| \widehat{H}_k P_k - P_{k'} \right\|_2^2. \quad (21)$$

In this study, a dense field forgery location algorithm (Li and Zhou, 2019) is employed. For each feature point in $\mathcal{M}_H$, local circular dubious field is defined as

$$r_k = \tau \sigma_k, \quad (22)$$

where $\tau$ denotes a paremeter (here, $\tau = 16$). Two dubious regions $S$ and $S'$ are established for matched feature point pairs in $\mathcal{M}_H$. Dubious regions are refined by color information, and each feature point in $S$ is defined as

$$P_* = \widehat{H}_k P_k, \quad P_k \in S. \tag{23}$$

In Equation (23), if the color vectors of $P_k$ and $P_*$ are close, they might be copy-move feature points, i.e., $P_k$ is the original feature point and $P_*$ is a copy-move forgery feature point. Let $Q_1$ be the set containing all the matched feature points in $S$, i.e.,

$$Q_1 = \{P_k, P_* | \max(|R(P_k) - \overline{R(P_*)}|, |G(P_k) - \overline{G(P_*)}|, |B(P_k) - \overline{B(P_*)}|) < Z_{rgb}\}, \quad P_k \in S, \tag{24}$$

$$\overline{W(P_*)} = \sum_{P_k \in \Omega(P_k)} W(P_k)/V, \; W \in \{R, G, B\}, \tag{25}$$

where $R(P_k)$, $G(P_k)$, and $B(P_k)$ denote the RGB values of feature point $P_k$, $V$ denotes a normalization factor, $\Omega(P_k)$ denotes a $3 \times 3$ patch centered at $P_k$, and $Z_{rgb}$ denotes a parameter (here, $Z_{rgb} = 10$).

On the other hand, each point in $S'$ is defined as

$$P'_* = \widehat{H}_k^{-1} P_{k'}, \qquad P_{k'} \in S'. \tag{26}$$

Similarly, let $Q_2$ be the set containing all the matched feature points in $S'$. If a feature point belonging to $Q_1 \cup Q_2$, this feature point will be marked as forgery feature point $A_{forgery}(x, y)$. The above procedure is iterated (here, 15 iterations) to find all the forgery feature points. Then, all the forgery feature points are grouped as forgery regions. To make forgery regions more accurately, morphological close operator is used to obtain the final forgery regions $A_{final}(x, y)$ in the image.

## 3 EXPERIMENTAL RESULTS

The proposed approach has been implemented on an Intel Core i7-7700K 4.20 GHz CPU with 32GB main memory for Windows 10 64-bit platform using MATLAB 9.4 (R2018a). To evaluate the effectiveness of the comparison and proposed approaches, FAU dataset (Christlein, et al., 2012) and CMH1 dataset (Silva, et al., 2015) are employed. FAU dataset consists of 48 high-resolution uncompressed PNG color images, whereas CMH1 consists of 23 copy-move forged images.

In this study, based on the final detected forgery region map and the ground truth map $GT$, $precision$ and $recall$ are employed as two performance metrics. Additionally, based on $precision$ and $recall$, $f_1$ score computed as

$$f_1 = 2 \times \frac{precision \times recall}{precision + recall}, \tag{27}$$

is employed as the third performance metric.

To evaluate the performance of the proposed approach, three comparison approaches, namely, Amerini, et al. (2013), Pun, et al. (2015), and Li, et al. (2019) are employed. The final detected forgery region maps of three comparison approaches and the proposed approach for two images of FAU dataset are shown in Figures 4 and 5. In terms of average $precision$, $recall$, and $f_1$ score, performance comparisons of the three comparison approaches and the proposed approach for FAU and CMH1 datasets are listed in Tables 1 and 2, respectively.

Table 1: In terms of average $precision$, $recall$, and $f_1$ score, performance comparisons of three comparison approaches and the proposed approach on FAU dataset.

| Approaches | $precision$ | $recall$ | $f_1$ score |
|---|---|---|---|
| Amerini, et al. (2013) | 0.359 | 0.887 | 0.455 |
| Pun, et al. (2015) | 0.966 | 0.655 | 0.753 |
| Li, et al. (2019) | 0.921 | 0.773 | 0.842 |
| Proposed | 0.938 | 0.815 | **0.859** |

Table 2: In terms of $precision$, $recall$, and $f_1$ score, performance comparisons of three comparison approaches and the proposed approach on CMH1 dataset.

| Approaches | $precision$ | $recall$ | $f_1$ score |
|---|---|---|---|
| Amerini, et al. (2013) | 0.942 | 0.935 | 0.940 |
| Pun, et al. (2015) | 0.929 | 0.920 | 0.924 |
| Li, et al. (2019) | 0.985 | 0.960 | 0.972 |
| Proposed | 0.978 | 0.972 | **0.975** |

Based on the experimental results listed in Tables 1 and 2, the proposed approach has good balances between precision and recall as well as larger $f_1$ scores, as compared with three comparison approaches. Based on the experimental results shown in Figures 4 and 5, the final detected forgery region maps of the proposed approach are better than those of three comparison approaches.

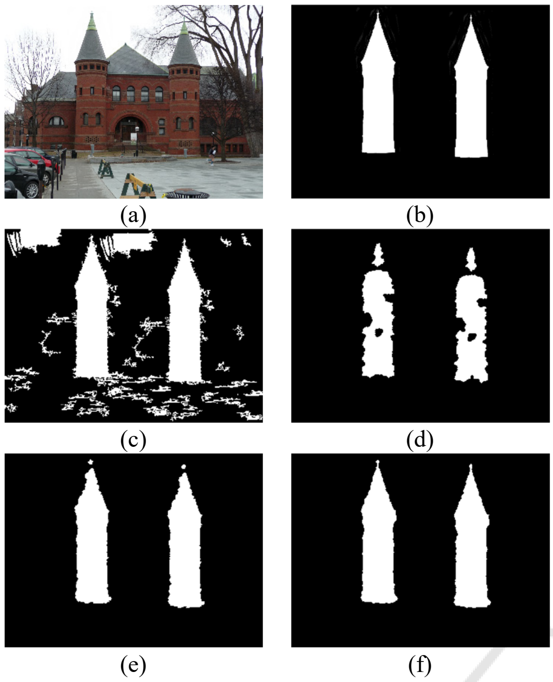

Figure 4: Final detected forgery region maps of “red_tower_copy” in FAU dataset: (a) original image; (b) ground truth, (c)-(f) the detected forgery region maps by Amerini, et al.’s approach (2013), Pun, et al.’s approach (2015), Li, et al.’s approach (2019), and the proposed approach.

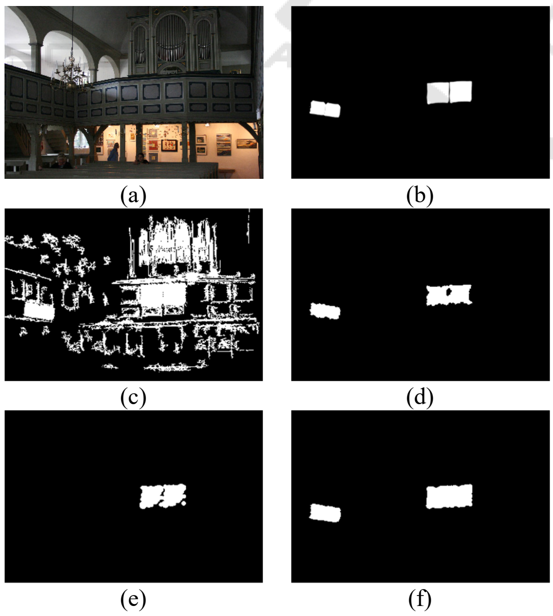

Figure 5: Final detected forgery region maps of “noise_pattern_copy” in FAU dataset: (a) original image; (b) ground truth, (c)-(f) the detected forgery region maps by Amerini, et al.’s approach (2013), Pun, et al.’s approach (2015), Li, et al.’s approach (2019), and the proposed approach.

# 4 CONCLUDING REMARKS

In this study, an image copy-move forgery detection approach using color features and hierarchical feature point matching is proposed. Based on the experimental results obtained in this study, the performance of the proposed approach is better than those of three comparison approaches.

# ACKNOWLEDGMENTS

This work was supported in part by Ministry of Science and Technology, Taiwan, ROC under Grants MOST 108-2221-E-194-049 and MOST 109-2221-E-194-042.

# REFERENCES

Amerini, I., Ballan, L., Caldelli, R., Del Bimbo, A., and Serra, G., 2011. A SIFT-based forensic method for copy-move attack detection and transformation recovery. In *IEEE Trans. on Information Forensics and Security*, 6(3), 1099-1110.

Amerini, I., et al., 2013. Copy-move forgery detection and localization by means of robust clustering with J-linkage. *Signal Processing: Image Communication*, 28(6), 659-669.

Bi, X., Pun, C. M., and Yuan, X. C., 2016. Multi-level dense descriptor and hierarchical feature matching for copy-move forgery detection. *Information Sciences*, 345, 226-242.

Chen, H., Yang, X., and Lyu, Y., 2020. Copy-move forgery detection based on keypoints clustering and similar neighborhood search algorithm. *IEEE Access*, 8, 36863-36875.

Christlein, V., et al., 2012. An evaluation of popular copy-move forgery detection approaches. *IEEE Trans. on Information Forensics and Security*, 7(6), 1841-1854.

Cozzolino, D., Poggi, G., and Verdoliva, L., 2015. Efficient dense-field copy–move forgery detection. *IEEE Trans. on Information Forensics and Security*, 10(11), 2284-2297.

Fadl, S. M. and Semary, N. A., 2017. Robust copy-move forgery revealing in digital images using polar coordinate system. *Neurocomputing*, 265, 57-65.

Gonzalez, R. C. and Woods, R. E., 2018. In *Digital Image Processing*, Prentice Hall. Upper Saddle River, NJ, 4th edition.

Huang, H. Y. and Ciou, A. J., 2019. Copy-move forgery detection for image forensics using the superpixel segmentation and the Helmert transformation. *EURASIP Journal on Image and Video Processing*, 1, 1-16.

Islam, A., Long, C., Basharat, A., and Hoogs, A., 2020. DOA-GAN: dual-order attentive generative adversarial network for image copy-move forgery detection and localization. In *IEEE/CVF Conf. on Computer Vision and Pattern Recognition (CVPR)*, 4675-4684.

Jin, G. and Wan, X., 2017. An improved method for SIFT-based copy move forgery detection using non-maximum value suppression and optimized J-linkage. *Signal Processing: Image Communication*, 57, 113-125.

Li, Y. and Zhou, J., 2019. Fast and effective image copy-move forgery detection via hierarchical feature point matching. *IEEE Trans. on Information Forensics and Security*, 14(5), 1307-1322.

Lin, X., et al., 2016. SIFT keypoint removal and injection via convex relaxation. *IEEE Trans. on Information Forensics and Security*, 11(8), 1722-1735.

Lowe, D. G., 2004. Distinctive image features from scale-invariant keypoints. *Int. Journal of Computer Vision*, 60(2), 91-110.

Pun, C., Yuan, X., and Bi, X., 2015. Image forgery detection using adaptive oversegmentation and feature point matching. *IEEE Trans. on Information Forensics and Security*, 10(8), 1705-1716.

Silva, E., et al., 2015. Going deeper into copy move forgery detection: exploring image telltales via multi-scale analysis and voting processes. *Journal of Visual Communication and Image Representation*, 29, 16-32.

Warif, N. B. A., et al., 2017. SIFT-symmetry: a robust detection method for copy-move forgery with reflection attack. *Journal of Visual Communication and Image Representation*, 46, 219-232.

Zhong, J. L. and Pun, C. M., 2020. An end-to-end Dense-InceptionNet for image copy-move forgery detection. *IEEE Trans. on Information Forensics and Security*, 15, 2134-2146.

Zhu, Y., et al., 2020. AR-Net: adaptive attention and residual refinement network for copy-move forgery detection. *IEEE Trans. on Industrial Informatics*, 16(10), 6714-6723.